Internal Ballistics of Spring Piston Airguns

Article · April 2015

CITATIONS
4

READS
10,413

1 author:

Domingo Tavella
Octanti Associates Inc
57 PUBLICATIONS **707** CITATIONS

SEE PROFILE

Internal Ballistics of Spring Piston Airguns

Domingo Tavella, Ph.D.

1.0 Summary

This work describes a comprehensive model of a spring piston airgun internal dynamics, where energy and momentum balance in the compression chamber and barrel are coupled with a finite element analysis of the spring. The problem is cast as a set of coupled non-linear ordinary differential equations, which are solved numerically. The model is applied under adiabatic conditions to a specific 4.5 mm caliber air gun, giving excellent agreement between measured and predicted performance.

2.0 Introduction

Air guns rely on a high-pressure gas source to propel a projectile. The gas is almost always air (hence the name), and the pressure source may be a tank of pre-compressed gas, or a compression chamber where gas is compressed by a piston propelled by a compressed steel spring. This latter type is the kind of air gun I will consider in this work.

A steel spring piston air gun can serve as an excellent workbench where any undergraduate student with a reasonable background in thermodynamics and calculus can put his or her understanding of conservation equations, ordinary differential equations, and elementary numerical analysis to the test.

While the main objective of this work is educational, the solution implemented here is, to my knowledge, the most comprehensive available in the open literature and can provide interesting insights into the workings spring-powered airguns. These insights are valuable in the design, repairs, and modifications of air guns.

Air guns - or more generally gas guns - come in many configurations and power levels, from BB smoothbore guns suitable for children all the way to hyper-velocity helium cannons, used in crater formation research, capable of propelling projectiles at hypersonic speeds.

In this work the focus is on conventional spring power air guns. Conventional means the spring is a standard steel round spring, as opposed to springs that rely on compressed gases, much like shock absorbers in automobiles. Within conventional spring powered air guns there are several possible configurations. The most common configuration consists of a single spring which is compressed when the gun is cocked. The compressed spring acts on a piston, and when the gun is fired the trigger releases the spring which in its turn propels the piston forward, compressing air in a compression chamber. The compression chamber communicates with the breech, where the projectile is seated, through a so-called transfer

port, which delivers high pressure air to the breech and this in turn propels the projective down the barrel[1].

The figure below illustrates the concept of a conventional spring-powered air gun. The figure is highly stylized and not to scale. The top illustration shows the gun action in the cocked position, where the piston is held in place by the trigger sear (the sear and its connection to the trigger blade are greatly simplified, triggers are far more complex than shown in the figure). The bottom illustration shows the gun action after firing and before the projectile has travelled all its way to the muzzle of the barrel.

FIGURE 1. Stylized schematic of a conventional spring piston air gun action - the trigger mechanism is highly simplified.

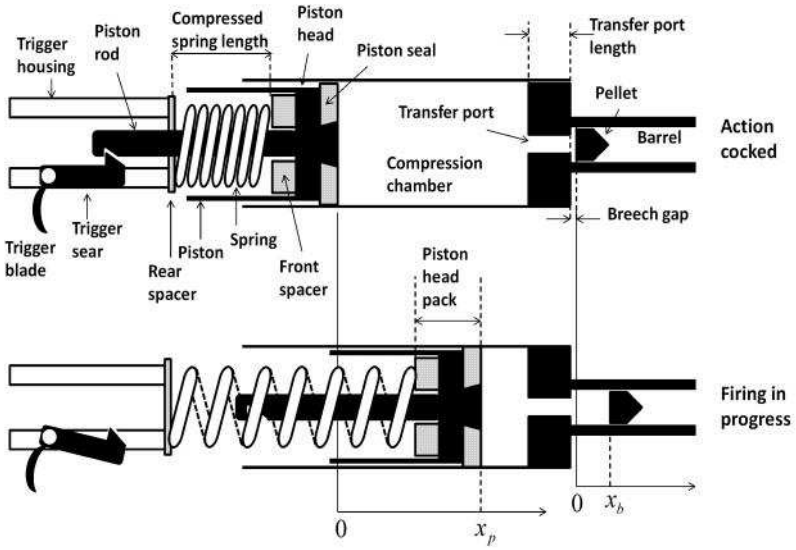

As the figure shows, the spring acts on the inside of a piston, pushing it forward. In many cases, the front part of the spring contacts a spacer, usually in the form of a "top hat" component (for simplicity, the drawing shows a simple thick washer rather than a top hat piece), while the rear of the spring contacts a spacer in the form of a flat washer. The role of the front spacer is to stabilize the spring and to add to the overall weight of the piston. The role of the rear spacer (there may be more than one) is to control the deflection energy stored by the spring.

The front of the piston is fitted with a seal, usually of synthetic material, designed to make air-tight contact with the inner wall of the compression chamber. The cocking rod is solidly attached to the piston[2].

I will refer to the piston itself, its attached cocking rod, the front spacer, and the piston seal as the piston assembly. The mass of the piston assembly, and to some extent the mass of the

1. Other configurations are possible, such as two pistons moving in opposite directions.
2. In many cases there is no cocking rod and the sear engages the piston directly - this detail is not important to the analysis.

spring itself, are important parameters in determining the gun's performance (by performance I mean the energy imparted to the projectile).

High pressure air is routed to the breech through a transfer port. The transfer port connects the breech with the compression chamber through the transfer channel. A typical diameter for the transfer port is about three millimeters and a typical length of the transfer channel is about twenty millimeters in length. In the figure above, the transfer port is shown centered with the compression chamber. This is not always the case, but the precise location of the transfer port is not important in our framework of analysis.

Relatively small spaces, that a simpler analysis would neglect, are important for proper accounting of energy balance in the compression chamber. Those small spaces are the transfer channel volume, any empty space associated with the seal design, and the breech gap (or sitting depth of the pellet), as the figure above illustrates.

In practice, the piston seal front face is not perfectly flat and often not perfectly solid. The most common seal design, referred to as parachute seal, has a relatively thin skirt separated by a narrow circular slot from the main body of the seal, as illustrated in the figure below. The purpose of this design is to insure tight contact with the pressure chamber wall. It is straightforward to take into account the effect of the annular empty space in the para-chute seal through a slight enlargement of the compression chamber, as I will discuss below.

FIGURE 2. Parachute seal and piston head longitudinal cross-section (not to scale).

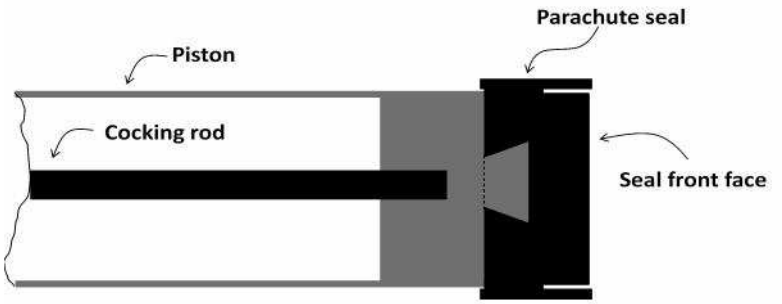

When the gun is fired, the piston moves forward compressing the air in the compression chamber. The pellet doesn't start to move until the piston has travelled significantly into the chamber - this typically takes a few milliseconds. A short time after the pellet begins to move down the barrel, the piston typically bounces backwards. This bounce happens when the pellet has moved a relatively short distance down the barrel and it usually causes high pressure air to be drawn back into the chamber. The pellet continues to accelerate even after the piston completes its forward motion, due to expansion of the air within the barrel behind the pellet, as well as due to air remaining in the chamber. The entire firing process until the pellet leaves the barrel takes between eight to ten milliseconds to complete.

From an efficiency point of view, a spring piston air gun is a relatively inefficient device. Typically, less than 30% of the energy initially stored in the spring converts into kinetic energy of the pellet. Some of the remaining energy is dissipated as friction, some is lost as

heat conduction, some is retained in the chamber, some is expelled from the barrel after the pellet leaves, etc. The precise understanding of the energy balance during the firing cycle is one of the primary goals of this work.

Modeling framework. The internal dynamics of spring piston air guns can be addressed at several levels of complexity. At the most comprehensive level, the analysis would involve solving the full compressible Navier-Stokes equations in the chamber and barrel, coupled with a detailed finite elements analysis of the spring, and would even include the pellet skirt pressure deformation and gas dynamics of air exiting the barrel during firing.

The most elementary approach would be to simply consider global energy and momentum conservation, making appropriate assumptions about thermal and frictional losses.

At an intermediate level of complexity, a control volume approach can capture the non-stationary thermodynamic exchanges between the several spaces within the air gun action, such as chamber, barrel, and transfer port channel, and couple this thermodynamic analysis with a suitable model of the spring plus piston. At this level of complexity, you capture the dynamics of the mechanical components (spring, piston, and pellet), as well as the time-dependent thermodynamics of the gas, but neglect the gas dynamic effects. The assumption of quasi-stationarity means inertia effects of the compressed gas are neglected, which implies thermodynamic balance and mass conservation are enough to solve the gas' time-dependent properties. This is the methodology I implement here, supplemented with an ad-hoc assumption about the behavior of kinetic energy behind the pellet. This assumption, as I will explain below, introduces a (hopefully minor) inconsistency in the conservation equations behind the pellet and allows us to estimate the order of magnitude of the kinetic energy of the air behind the pellet.

I will not make any explicit assumptions about the air undergoing any specific form of polytropic process. This approach can deal with heat losses and heat generation (as is the case of lubrication combustion) as primary quantities you can infer from calibration. At the same time, this approach is powerful enough to capture the effects on performance of spring mass, transfer port length and diameter, and pellet seating depth, among other things.

Previous work. A small number of papers have been published describing mathematical models of air guns, and even fewer dealing with spring piston air guns. Except for one, these reports deal with pre-compressed pneumatic air cannons, not with spring-powered air guns.

Compton (Ref. 1) considered a spring piston air rifle model under the assumption of isothermal compression. Compton's model doesn't account for the dead spaces within the compression chamber, transfer port, and the space between the breech and the pellet base. The fact that the firing cycle last less than one hundreds of a second, evidence of seal erosion due heating, and considerations of heat transfer from gases under pressure suggest the isothermal assumption is unlikely to hold in practice.

Mungan (Ref. 2) analyzes a potato gun under the adiabatic expansion assumption. The adiabatic expansion is justified on the basis that the potato cannon is not made of metal.

Denny (Ref. 3) considers a pneumatic air cannon under the isothermal assumption, in contrast to Mungan's analysis, Rohrbach et al. (Ref. 4) also consider a pneumatic air canon and conclude that neither the isothermal nor the adiabatic assumptions are fully satisfactory.

This work differs from and adds to the existing literature in at least three important ways. First, this analysis includes complexities such as dead spaces in the seal, transfer port, and breech, whose importance must be inferred from computational results, rather than assumed away. Second, by allowing for heat conduction into the compression chamber walls this model is not constrained by adiabatic, isothermal, or polytropic restrictions. Third, the spring itself is dealt with a simple finite element method, which allows for the capture elements of spring vibration and surge.

3.0 Modeling approach

In a spring-powered airgun action you can distinguish seven areas involved in energy, mass and momentum transfer: 1) the spring plus piston assembly, 2) the compression chamber, 3) cavities in the piston seal, 4) the transfer port channel, 5) the space in the barrel between the breech and back of the pellet, 6) the pellet itself, and 7) the space in the barrel between the pellet nose and the muzzle. I will derive a set of coupled ordinary differential equations connecting the piston position, the air state variables, and pellet position during the firing cycle. I will make the following modeling assumptions.

Spring piston assembly. I will model the spring piston assembly as a spring mass system, where the mass is subjected to external forces. The spring mass has a significant effect on performance, and that proper capture of the spring mass effect can be achieved with a finite element model of the spring-piston assembly.

Compression chamber. I will assume the process is quasi-stationary and uniform, which means the kinetic energy component can be neglected compared with the thermal energy. The model will allow for heat transfer through the walls.

Seal cavities. Spaces within the piston seal will be dealt with as corrections to the chamber volume.

Transfer port channel. The transfer channel plays a role in that hot, high-pressure air will remain trapped in it as the pellet moves down the barrel. As a result, the length of the channel significantly affects performance and cannot be neglected. Importantly, the length of the transfer channel influences the transfer port diameter that maximizes performance.

Breech gap. The space between the transfer port plane and the pellet base (determined by how deeply into breech the pellet sits) will be modelled as a correction to the breech-to-pellet volume in the barrel.

Breech to pellet base. Energy is transferred from the compression chamber to the space between the breech and the pellet base through the transfer port. I will take into account the gas kinetic energy through a simple ad-hoc assumption (which, as mentioned earlier, introduces some

inconsistency in the conservation equations. As it will turn out, the gas kinetic energy in their region is not important and can be neglected without major impact on performance.

Pellet. I will model the pellet as a mass of the same diameter as the breech, subjected to four kinds of forces: pressure forces that accelerate the pellet, friction forces originating in the pellet skirt, friction forces due to elastic compression of the pellet, and friction forces due to interaction of the pellet with the rifling lands.

Pellet nose to muzzle. Here energy is transferred to the column of air in front of the pellet. I will assume the gas is incompressible in this region. This is not an important component of the overall balance.

3.1 Connecting the pieces

In their simpler set up, Compton (Ref. 1) and Denny (Ref. 3) manage to get analytical expressions for the pellet velocity as a function of chamber pressure (Compton), and spring and chamber parameters (Denny). Getting closed form solutions in our case, where you allow for additional complexities, would be much harder. Rather than attempting to reduce the problem analytically, it is easier and more flexible to solve the various components (spring, chamber, and barrel plus pellet) numerically in time, allowing the components to communicate through state and position variables. Doing this reduces the chance of error, and makes it possible to extend the model to include lubricant combustion. In addition, from a computational view, the problem naturally breaks down into components that lend themselves to object programming[1].

4.0 Modeling the spring

You can model the spring at various levels of complexity. The simplest thing to do is to idealize the spring piston combination as a spring mass system with the mass concentrated at a point. A more comprehensive approach is to resolve the deflection of the actual coils of the spring.

4.1 Simplified approaches

Massless spring. This is the simplest model of a mass-spring system. A massless spring with stiffness k, free length h, and a piston with mass M_p, acted on by a friction force F_f in direction opposite to the piston velocity, and by a pressure force $A_p(p_c - p_a)$, where A_p is the piston seal area (equal to the compression chamber cross-sectional area), p_c is the absolute pressure in the chamber, and p_a is the atmospheric pressure, follows the equation

1. The spring, compression chamber, and bore can be represented as objects that communicate with each other through position (spring), and thermodynamic variables (compression chamber and bore).

$$\frac{dv_p}{dt} = \frac{k}{M_p}(h - x_s) - \frac{1}{M_p}[A_p(p_c - p_a) + \mathrm{sgn}(v_p)F_f] \quad \text{(EQ 1)}$$

where v_p is the piston velocity, x_S is the front end position of the spring, and where I assume one side of the piston head is exposed to the chamber pressure while the opposite side is exposed to atmospheric pressure. Notice that the piston position, x_p is not the same as the spring front end position, x_s; they differ by the seal thickness and the top hat spacer thickness.

Mass-corrected spring. In a typical airgun, the mass of the spring can be as large as one third of the mass of the piston assembly. If you can assume that the relative spacing of the spring coils remains uniform as the spring undergoes longitudinal deflection, it is straightforward to correct for the mass in the spring-piston system to account for the spring mass. This correction insures that the kinetic energy of the spring-mass combination accounts for the kinetic energy of the spring itself. The correction consists in adding one third of the spring mass to the piston assembly mass (Ruby (Ref. 5).) If the mass of the spring is m_s, the corrected equation of motion is

$$\frac{dv_p}{dt} = \frac{k}{M_p + \frac{1}{3}m_s}(h - x_s) - \frac{1}{M_p + \frac{1}{3}m_s}[A_p(p_c - p_a) + \mathrm{sgn}(v_p)F_f] \quad \text{(EQ 2)}$$

The validity of this equation hinges on the assumption of uniform spring deflection. This assumption may become questionable when the piston reaches the end of the chamber and bounces backwards. Calculations show that the kinetic energy retained by the spring when the firing cycle ends is higher than suggested by the mass correction, and as a result, the mass-corrected approach overestimates the power of the gun.

4.2 Spring finite element approach

Figure 1 shows a simple finite elements model of the spring. The spring is divided into n segments, each with mass m and each with the same number of coils (where the number of coils can be non-integer). Time functions $x^i(t)$ denote the horizontal positions of masses m. At the right end of the spring is a mass M which is acted on by an external force F.

Denoting the initial uniform spacing between masses by Δ, the forces due to spring deflection acting on the left and right sides of mass located at $x^i(t)$ are given by the formulas (time argument omitted for simplicity)

$$F_l^i = k[\Delta - (x^i - x^{i-1})] \quad \text{(EQ 3)}$$

$$F_r^i = -k[\Delta - (x^{i+1} - x^i)] \quad \text{(EQ 4)}$$

If the spring segment on the left side of the mass shrinks, F_l is positive. If the spring segment on the right side of the mass shrinks, F_r is negative.

The net deflection force acting on the mass located at $x^i(t)$ is the sum of left and right forces, plus any friction forces. This causes the initial mass spacings to cancel out.

$$F_l^i + F_r^i = k[\Delta - (x^i - x^{i-1})] - k[\Delta - (x^{i+1} - x^i)] \quad \text{(EQ 5)}$$

$$F_l^i + F_r^i = k(x^{i-1} - 2x^i + x^{i+1}) \quad \text{(EQ 6)}$$

If v^i is the velocity of the mass located at $x^i(t)$, momentum conservation gives us a system of ordinary differential equations.

FIGURE 3. Finite element spring model (friction forces F_f not shown for clarity).

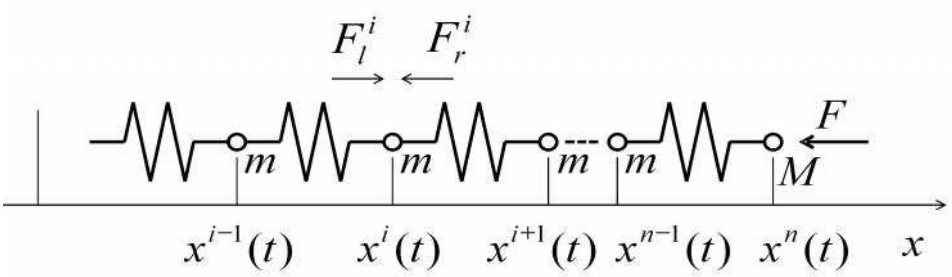

Excluding the first and last coordinate points, the system of ordinary differential equations (ODE) is as follows

$$\frac{dv^i}{dt} = \frac{k}{m}(x^{i-1} - 2x^i + x^{i+1}) + \text{sgn}(v^i)\frac{F_f^i}{m}, \quad i = 1, 2, \ldots, n-1 \quad \text{(EQ 7)}$$

$$\frac{dx^i}{dt} = v^i \quad \text{(EQ 8)}$$

Here F_f^i is a friction force acting on the i^{th} mass element. I will assume the left end of the spring is stationary, namely $x^0(t) = x_0$. The ODE for the first spring mass is therefore

$$\frac{dv^1}{dt} = \frac{k}{m}(x_0 - 2x^1 + x^2) + \text{sgn}(v^1)\frac{F_f^1}{m} \quad \text{(EQ 9)}$$

The ODE for mass M is

$$\frac{\mathrm{d}v^n}{\mathrm{d}t} = \frac{k}{M}[\Delta - (x^n - x^{n-1})] - \frac{F_f^n + F}{M} \qquad \text{(EQ 10)}$$

where F_f^n is the sum of the friction forces acting on the n^{th} element and the piston seal, and F results from pressure forces acting on both sides of the piston seal. The next equation shows this system in matrix form. For $n = 4$ and defining $\zeta = \frac{k}{n}$ and $\zeta_M = \frac{k}{M}$, the system for the element velocities looks as follows (notice the last row has no factor of 2, this is because the piston mass is at the very end of the spring).

$$\frac{\mathrm{d}}{\mathrm{d}t}\begin{bmatrix} v^1 \\ v^2 \\ v^3 \\ v^4 \end{bmatrix} = \begin{bmatrix} -2\zeta & \zeta & 0 & 0 \\ \zeta & -2\zeta & \zeta & 0 \\ 0 & \zeta & -2\zeta & \zeta \\ 0 & 0 & \zeta & -\zeta_M \end{bmatrix}\begin{bmatrix} x^1 \\ x^2 \\ x^3 \\ x^4 \end{bmatrix} + \begin{bmatrix} \zeta x_0 - \mathrm{sgn}(v^1)\frac{F_f^1}{m} \\ -\mathrm{sgn}(v^2)\frac{F_f^2}{m} \\ -\mathrm{sgn}(v^3)\frac{F_f^3}{m} \\ \zeta_M \Delta - \mathrm{sgn}(v^4)\frac{F_f^4 + F}{M} \end{bmatrix} \qquad \text{(EQ 11)}$$

This system will communicate with the compression chamber thermodynamics through the force term F. This is a tridiagonal system for the accelerations of the finite elements masses. This system can be solved extremely efficiently.

Spring stiffness. With G the sheer modulus of elasticity, R_s the spring mean radius, D_w the wire diameter, and N_a the number of active coils, the overall spring stiffness coefficient, k_a, is (Deutchman et al, Ref(6))

$$k_a = \frac{GD_w^4}{64N_aR_s^3} \qquad \text{(EQ 12)}$$

For springs as you typically find in air guns the number of active coils is the total number of coils, N_t, minus two, assuming the end coils are flattened and ground.

$$N_a = N_t - 2 \qquad \text{(EQ 13)}$$

If there are n spring segments, and since the stiffness is inversely proportional to the number of active coils, each segment has a stiffness given by

$$k = nk_a \qquad \text{(EQ 14)}$$

Spring mass discretization. If there are n spring segments, the number of coils in each segment is

$$\Delta N_a = \frac{N_a}{n} \quad \text{(EQ 15)}$$

Each spring segment has mass

$$m_s = \frac{\pi^2 D_w^2 \rho_s R_s N_a}{2n} \quad \text{(EQ 16)}$$

where ρ_s is the density of the spring metal.

Element masses. The spring segments masses are allocated to the finite element model as shown in the following figure.

FIGURE 4. Spring mass segment allocation.

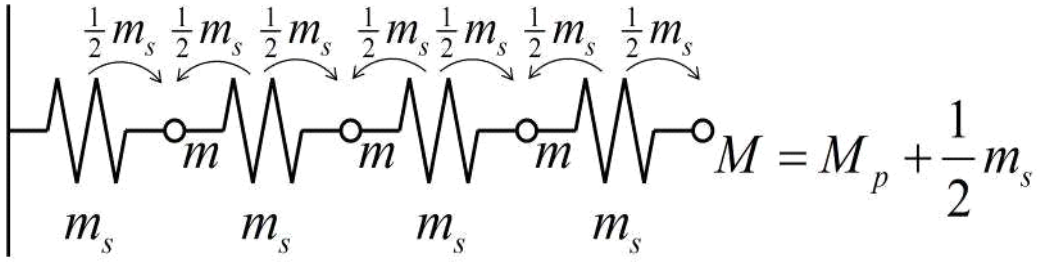

Here M_p is the piston mass. Therefore, the quantities ζ and ζ_M are given by the formulas

$$\zeta = m_s \quad \text{(EQ 17)}$$

$$\zeta_M = M_p + \frac{1}{2}m_s \quad \text{(EQ 18)}$$

5.0 Compression chamber

The model for the compression chamber is designed to incorporate both cavities or pockets in the seal itself, where high-pressure air can remain trapped when the firing mechanism is triggered, as well as the transfer port channel, which will retain some of the high pressure air during firing. The figure below shows the compression chamber model geometry.

While it is clear that seal cavities can be handled by an effective change in the chamber volume, the transfer channel requires closer attention. If you view the transfer channel as a separate component of your system, you find that the transfer channel cannot be handled with

thermodynamic considerations alone. This is because the channel doesn't have moving boundaries. As a result, dealing with the transfer channel as a separate component requires solving a fluid dynamic problem, where you take into account entrance conditions and viscous effects, significantly adding to the complexity of the solution.

You can make two approximations to handle the transfer channel with thermodynamic considerations only. One approximation is to assume you can enlarge the compression chamber volume by the volume of the transfer channel. Under quasi-stationary conditions this approximation would be exact if the mass and energy densities in the transfer channel were identical to the mass and energy densities in the compression chamber. Another approximation is to assume the density and energy within the channel are uniform and equal to their exit (or discharge) values.

These two approximations give very similar results, but their implementation is very different. Here I will only consider the first approximation. As shown in the next figure, the front face of the piston is assumed to have an infinitesimally thin lip of depth δ. To implement the first approximation, you choose δ such that volume $\frac{\pi}{4}D_p^2\delta$, where D_p is the piston diameter, equals the transfer channel volume plus the volume of the seal cavities or cavities accounting for the uneven front seal surface, and otherwise ignore the transfer channel in your conservation equations.

FIGURE 5. Compression chamber model - subscript "a" refers to atmospheric conditions, subscript "c" refers to compression chamber conditions, and subscript "d" refers to transfer port discharge conditions.

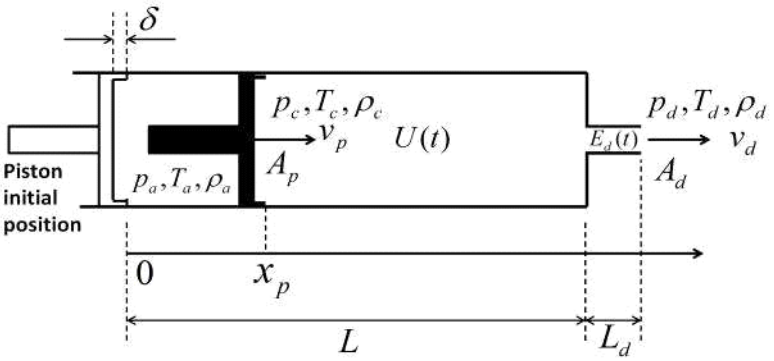

Transfer port discharge values. The discharge pressure is the starting point to compute the thermodynamic values at the transfer port plane. Ignoring the kinetic energy within the compression chamber, the critical value of the breech pres-sure below which the flow at the transfer port becomes sonic is

$$p_d^* = p_c\left(\frac{2}{\gamma+1}\right)^{\frac{\gamma}{\gamma-1}} \qquad \text{(EQ 19)}$$

where γ is the ratio of specific heats, $\gamma = \frac{c_p}{c_v}$. Ignoring the kinetic energy amounts to assuming the compression chamber pressure, p_c, equals the stagnation pressure. This assumption is justified if the kinetic energy of the air in the compression chamber is much smaller than its thermal energy.

If the breech pressure is greater than p_d^* (but less than the chamber pressure), the flow at the transfer port is subsonic and the Mach number results from assuming isentropic expansion,

$$M_d^2 = \frac{2}{\gamma - 1}\left[\left(\frac{p_c}{p_d}\right)^{\frac{\gamma-1}{\gamma}} - 1\right] \quad \text{(EQ 20)}$$

where p_d is set equal to the breech pressure. If the breech pressure is less than p_d^*, the Mach number is one, and $p_d = p_d^*$ [1]. If the breech pressure is greater than the chamber pressure, the flow reverses and air flows back into the compression chamber.

Once the pressure is known, the transfer port discharge temperature follows from assuming isentropic expansion[2],

$$T_d = T_c\left(\frac{p_d}{p_c}\right)^{\frac{\gamma-1}{\gamma}} \quad \text{(EQ 21)}$$

where T_c is the chamber temperature. With this, the speed of sound at discharge is

$$c = \sqrt{\gamma R T_d} \quad \text{(EQ 22)}$$

where *R* is the gas constant (air in our case). The mass flow per unit area follows form (notice there is a "dot" on top of the "*m*"),

$$\dot{m} = M_d c \rho_d \quad \text{(EQ 23)}$$

where ρ_d is the transfer port discharge density. Since $A_d v_d \rho_d = C_d A_d \dot{m}$, where C_d is a discharge coefficient, the discharge velocity is

1. Computations for the air gun used as experimental validation of this model suggest the Mach number at the transfer port is less than one.
2. The isentropic expansion formula can be modified to account for the barrel diameter when air flows from the barrel into the compression chamber.

$$v_d = \frac{C_d \dot{m}}{\rho_d} \tag{EQ 24}$$

The discharge density comes from the state equation

$$\rho_d = \frac{p_d}{R T_d} \tag{EQ 25}$$

Working with the conservation equations, I will get ordinary differential equations for the chamber density and temperature, with the pressure computed from the state equation. To account for the transfer port mass and energy, I will apply the second approximation I discussed earlier, which explicitly accounts for the transfer port mass and energy.

Conservation of mass. The rates of change of mass in the chamber and transfer port channel must be balanced by the mass discharge into the breech.

$$\frac{\mathrm{d}}{\mathrm{d}t}[A_p(L + \delta - x_p)\rho_c] = -C_d \dot{m} A_d \tag{EQ 26}$$

where A_p is the compression chamber cross-sectional area and x_p is the piston position (see Figure 5). This gives us an ordinary differential equation for the chamber density.

$$\frac{\mathrm{d}\rho_c}{\mathrm{d}t} = \frac{-C_d \eta \dot{m} + \rho_c v_p}{L + \delta - x_p} \tag{EQ 27}$$

with v_p the piston velocity.

Energy balance. Neglecting the kinetic energy component in the chamber, the rate of thermal energy change in the chamber must equal the rate of energy input from the piston displacement minus the convection of enthalpy and kinetic energy out the transfer port, minus the heat lost to the surrounding environment,

$$\frac{\mathrm{d}}{\mathrm{d}t}[A_p(L + \delta - x_p)\rho_c c_v T_c] = A_p p_c v_p - C_d \dot{m} A_d \left(\frac{1}{2} v_d^2 + c_p T_d\right) - \frac{\mathrm{d}Q}{\mathrm{d}t} \tag{EQ 28}$$

where $\frac{\mathrm{d}Q}{\mathrm{d}t}$ is the rate of heat lost to the environment. A little algebra gives us an ODE for the chamber temperature.

$$\frac{\mathrm{d}T_c}{\mathrm{d}t} = \frac{p_c v_p - C_d \eta \dot{m}\left(\frac{1}{2} v_d^2 + c_p T_d - c_v T_c\right) - \frac{1}{A_p}\frac{\mathrm{d}Q}{\mathrm{d}t}}{(L + \delta - x_p)\rho_c c_v} \tag{EQ 29}$$

Heat lost to the environment. Ignoring the heat lost within the transfer channel, the rate of heat lost to the environment is proportional to the product of the chamber wall surface

and the temperature difference between the gas inside the chamber and the chamber wall, namely

$$\frac{\mathrm{d}Q}{\mathrm{d}t} = \mu\left[\pi D_p(L - x_p) + \frac{\pi}{4}D_p^2\right](T_c - T_a) \qquad \text{(EQ 30)}$$

where T_a is the atmospheric temperature, D_p is the piston diameter (same as the compression chamber diameter) and μ is a heat transfer coefficient. Here I assume the chamber walls are at atmospheric temperature. The connection between the chamber and the spring is through the pressure force on the piston - in absolute value this force is

$$F = (p_c - p_a)A_p \qquad \text{(EQ 31)}$$

where p_a is the atmospheric pressure. This is the force term that appears in the last equation in the finite elements ODE system.

5.1 Barrel and pellet

The next figure shows the configuration of the barrel and pellet. The pellet position, x_b, is measured starting from a distance x_0 from the transfer port. This distance accounts for the sitting depth[1] of the pellet into the breech, and for any spacing between the breech and the transfer port. This distance, as it turns out, is important thermodynamically and it influences the numerical conditioning of the differential equations that describes the problem.

To derive the conservation equations I will consider a control volume that extends from the plane of the transfer port to the base of the pellet. As was the case with the compression chamber, I will introduce the simplifying assumption that there are no density, pressure, or temperature gradients between the breech and the pellet base.

In order to estimate the importance of the kinetic energy of the column of air behind the pellet, however, we must make an assumption about the distribution of air velocity behind the pellet. A common approximation in the internal ballistics of fire arms, known as the Lagrange gradient approximation - see Carlucci and Jacobson (Ref. 7) or Morrison et al (Ref. 8) - leads to the result that, if the gas behind the projectile has uniform density, the gas velocity varies linearly from the breech to the base of the projectile. This assumption, however, is not consistent with assuming that the temperature and pressure are also uniform behind the projectile, which is our framework here.

To be perfectly consistent, the Lagrange gradient approximation has to be specialized to the conditions we find in an airgun, which would require relaxing the assumption of state uniformity behind the pellet.

1. By seating depth I mean the distance between the rear end of the pellet and the breech seal plane.

Rather than relaxing the assumption of state uniformity behind the pellet, I will introduce the ad-hoc assumption that a linearly varying air velocity distribution behind the pellet can be used to assess the extent to which kinetic energy behind the pellet is important. As it turns out, under this assumption it is not important.

FIGURE 6. Barrel and pellet.

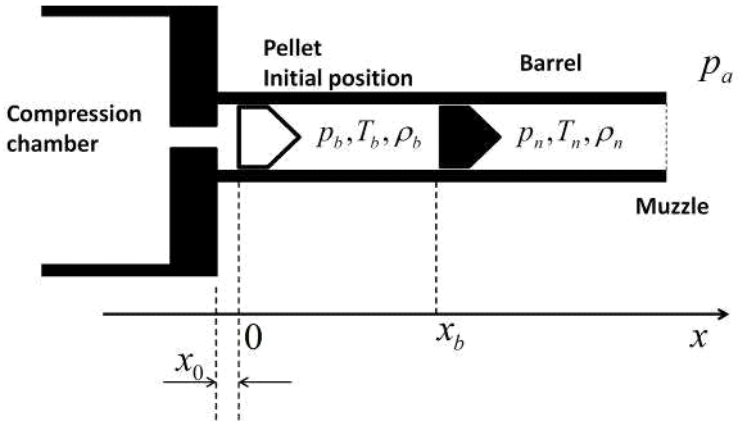

Mass conservation. Change in gas mass behind pellet equals mass flow into breech

$$\frac{\mathrm{d}}{\mathrm{d}t}[(x_0 + x_b)\rho_b] = C_d \eta_b \dot{m} \qquad \text{(EQ 32)}$$

where $\eta_b = \dfrac{A_d}{A_b}$ is the discharge port-breech constriction ratio and subscript b stands for breech. Under the uniformity assumption, you only have to worry about total time derivatives.

$$\frac{\mathrm{d}\rho_b}{\mathrm{d}t} = \frac{C_d \eta_b \dot{m} - v_b \rho_b}{x_0 + x_b} \qquad \text{(EQ 33)}$$

where $v_b = \dfrac{\mathrm{d}x_b}{\mathrm{d}t}$ is the pellet velocity.

Energy. The sum of the changes in internal and kinetic energy of the gas behind the pellet equals the enthalpy plus kinetic energy inflows through the transfer port, minus the work done by the air on the base of the pellet, minus the heat lost to the barrel. Note that the pellet friction doesn't enter into this balance because the control volume doesn't include the pellet itself. Assume $x \geq 0$ describes pellet position in barrel, and the starting position of the pellet is a distance x_0 from the breech plane (pellet coordinate x_b is measured from x_0),

$$\frac{\mathrm{d}}{\mathrm{d}t}[A_b(x_0+x_b)\rho_b c_v T_b]+\frac{\mathrm{d}}{\mathrm{d}t}KE = C_d A_d \dot{m}\left(c_p T_d+\frac{1}{2}v_d^2\right)-p_b A_b v_b-\frac{\mathrm{d}Q_b}{\mathrm{d}t} \qquad \text{(EQ 34)}$$

where KE stands for the kinetic energy of the gas in the volume between the transfer port and the pellet base, and $\frac{\mathrm{d}Q_b}{\mathrm{d}t}$ is the rate of heat lost from the barrel behind the pellet to the environment. A little algebra gives us the ODE for the breech temperature,

$$\frac{\mathrm{d}T_b}{\mathrm{d}t} = \frac{C_d \eta_b \dot{m}\left(c_p T_d - c_v T_b+\frac{1}{2}v_d^2\right)-p_b v_b-\frac{1}{A_b}\frac{\mathrm{d}}{\mathrm{d}t}KE-\frac{1}{A_b}\frac{\mathrm{d}Q_b}{\mathrm{d}t}}{(x_0+x_b)\rho_c c_v} \qquad \text{(EQ 35)}$$

The kinetic energy term would complicate things if you wanted to capture the kinetic energy contribution to the same level of accuracy as the other thermodynamic quantities. The reason is that KE is an explicit function of the mass flow rate, $\dot{m}$. The mass flow rate is itself a function of the state variables in the chamber. This means that an expression for $\frac{\mathrm{d}}{\mathrm{d}t}KE$ would connect the ODEs of the chamber with the ODEs of the barrel through the time derivatives of the state variables, not just through the state variables values. This problem can be easily resolved by time-lagging the $\frac{\mathrm{d}}{\mathrm{d}t}KE$ term. As it turns out, in an air gun the influence of the gas kinetic energy is small and can be ignored. Let's now come up with a formulation for KE.

Kinetic energy behind the pellet. There is a fundamental issue in computing the kinetic energy of the gas behind the pellet under the uniformity assumption. Physical constraints require that the gas velocity must be non-uniform along the bore axis, and this is inconsistent with uniformity. One way to get around this issue is to make the ad-hoc assumption that the air velocity behind the pellet is linearly distributed between the breech and the pellet base, consistent with the gradient approximation mentioned earlier (Carlucci and Jacobson (Ref. 7)). This is consistent with uniform density, but is not consistent with uniformity of all variables. Despite this conflict, the assumption of velocity linearity will give us an idea of how important or unimportant the kinetic energy behind the pellet is.

In a firearm, under the Lagrange gradient approximation, the gas velocity behind the projectile expands linearly with zero velocity at the breech and the velocity of the projectile at the base of the projectile.

In an airgun, if the port is of the same diameter as the breech and assuming flow is not chocked within the barrel anywhere behind pellet, under the uniformity assumption the velocity of the gas would be equal to the pellet velocity.

The situation of interest is intermediate between these two scenarios. I will assume the velocity of the air varies linearly between the breech and the base of the pellet, where the

velocity at the breech is computed from continuity. If x_b is the current position of the pellet, and v_b is the current pellet velocity, the distribution of air velocity along the barrel between the breech and the pellet base can be described as follows,

$$v(x) = v_0 + (v_b - v_0)\frac{x}{x_b} \quad \text{(EQ 36)}$$

where v_0 is the velocity at the breech - from mass conservation, assuming mixing happens over a vanishingly short distance,

$$v_0 = \frac{C_d \dot{m} A_d}{\rho_b A_b} \quad \text{(EQ 37)}$$

The kinetic energy of the gas behind the pellet is

$$KE = \frac{1}{2} A_b \left[\int_{x_0}^{x_b} \rho_b v^2 dx + x_0 \rho_b v_0^2 \right] \quad \text{(EQ 38)}$$

Carrying out the integration,

$$KE = \frac{1}{6} A_b \rho_b [v_b^2 + v_0(v_b + v_0)] x_b + \frac{1}{2} A_b \rho_b x_0 v_0^2 \quad \text{(EQ 39)}$$

If the transfer port discharge velocity is zero, this expression agrees with the solution in Carlucci and Jacobson (Ref. 7).

Heat lost to barrel. Ignoring heat lost within the breach gap and the heat lost to the pellet itself, the rate of heat lost to the barrel, in a manner similar to the compression chamber, can be assumed to be proportional to the product of the barrel wall surface and the temperature difference between the gas inside the barrel and the barrel wall. Assuming the barrel is at ambient temperature,

$$\frac{dQ_b}{dt} = \mu \pi D_b x_b (T_b - T_a) \quad \text{(EQ 40)}$$

where D_b is the barrel diameter and μ is the same heat transfer coefficient I used in the compression chamber case. Consideration of heat loss to the barrel is added for completeness. Heat loss to the barrel is often ignored in internal firearm ballistics, and it is not actually needed in our case.

Momentum. The momentum equation applied to the pellet allows us to connect the pressure acting at the base of the pellet with the pellet position. The pressure forces acting on the pellet must balance forces due to inertia and friction. This balancing is accomplished by equating the work done by the pressures acting on the pellet base, p_b, and pellet nose, p_n,

to the sum of changes in the pellet's rotational and translational energies plus work dissipated by the pellet through friction. Note that change in energy of the air ahead of the pellet is not part of this balance.

The pellet momentum equation is therefore

$$A_b(p_b - p_n)\mathrm{d}x_b = \mathrm{d}\left(\frac{1}{2}m_b v_b^2\right) + \mathrm{d}\left(\frac{1}{2}I_b\omega^2\right) + G\mathrm{d}x_b \qquad \text{(EQ 41)}$$

where ω is the rotational angular velocity of the pellet, G is the friction force acting on the pellet, m_b is the pellet mass, and I_b is the pellet's axial moment of inertia. You can now link the rotational velocity with the twist rate, T_R, defined as $T_R = \frac{1}{L_R}$, where L_R is the distance over which the pellet describes one revolution.

The twist rate of firearms and airguns is usually constant, but it doesn't have to be. It is possible for the twist rate to vary along the length of the barrel, usually increasing along the barrel[1]. An extreme form of variable twist rate is one where the twist is present only in a section of the barrel[2]. Computations will show that in an airgun, as far as energy output is concerned, there is no advantage in using a partial-twist barrel. This doesn't mean that other advantages might not exist, such as a more favorable dynamic response by the gun-shooter assembly.

In what follows I will assume constant twist rate (the partial twist is trivial to implement). As a function of distance travelled, x_b, the pellet undergoes the number of revolutions

$$n_R = T_R x_b \qquad \text{(EQ 42)}$$

The number of revolutions per unit time is,

$$\frac{\mathrm{d}n_R}{\mathrm{d}t} = T_R v_b \qquad \text{(EQ 43)}$$

The angular velocity of the pellet is therefore

$$\omega = 2\pi T_R v_b \qquad \text{(EQ 44)}$$

With this, the momentum equation gives us the following equation for the pellet acceleration.

1. The idea of variable twist has been around for a very long time. Bartlein Barrels, a US manufacturer of precision barrels, markets a barrel with slowly increasing twist.
2. At least one airgun manufacturer markets a guns with partial twist barrels, where the twist is applied a few inches near the muzzle.

$$\frac{\mathrm{d}v_b}{\mathrm{d}t} = \frac{A_b(p_b - p_n) - G}{m_b + (2\pi T_R)^2 I_b} \qquad \text{(EQ 45)}$$

Friction and rifling forces. Friction force G is made up of three components. One is the elasticity friction due to pellet deformation - this component, denoted by G_n, is independent of the pressure acting on the base of the pellet. The second component is friction due to expansion of the skirt, G_s, and is dependent on the pressure behind the pellet. The third component, denoted by G_r, is due to friction by the pellet against the barrel lands.

$$G = G_n + G_s + G_r \qquad \text{(EQ 46)}$$

To visualize how the first two components of friction come about, consider the longitudinal cross-section of a typical low- to medium-powered air rifle, shown in the figure below. When the gun is fired, the high pressure acting on the pellet base causes the skirt to flatten against the barrel, developing a circular area of depth δ_s, which is acted on by friction force G_s. This friction force is a fraction of the force produced by the pressure acting on a ring of diameter D_b and depth δ_s, namely,

$$G_s = \mu p_b \pi D_b \delta_s \qquad \text{(EQ 47)}$$

where μ is an appropriate friction coefficient.

FIGURE 7. Typical low- to medium-power airgun pellet cross-section, before and after firing.

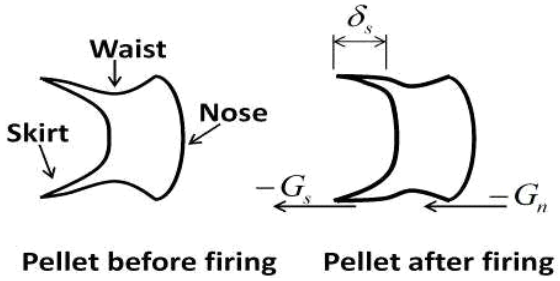

Given the shape of a standard low to medium power pellet, friction due to elastic deformation will be concentrated around the nose. Firearm bullets and some high-power airgun pellets, which look more like conventional bullets, differ in this regards, and are subjected primarily to elastic deformation friction. G_n is a constant for each pellet and is best determined by pushing a pellet through the barrel. To get an expression for the rifling force G_r, consider the sketch in the Figure 7. Due to rotational acceleration, the rifling exerts a force against the pellet, F_T, which is perpendicular to the pellet axis and can be decomposed into

two components, one perpendicular to the rifling, $\frac{F_T}{\cos\theta}$, and the other tangential to the rifling, $\mu\frac{F_T}{\cos\theta}$. This tangential component arises due to friction against the lands and gives rise to a longitudinal force, $G_r = \mu F_T$, that slows down the pellet advancement in the bore. To compute F_T consider the rotational torque T about the pellet axis,

$$F_T = \frac{T}{r} = \frac{1}{r} I_b \frac{d\omega}{dt} = \frac{2\pi T_R}{r} I_b \frac{dv_b}{dt} \qquad \text{(EQ 48)}$$

FIGURE 8. Forces acting on the pellet due to the barrel rifling - angle of rifling, θ, highly exaggerated for clarity.

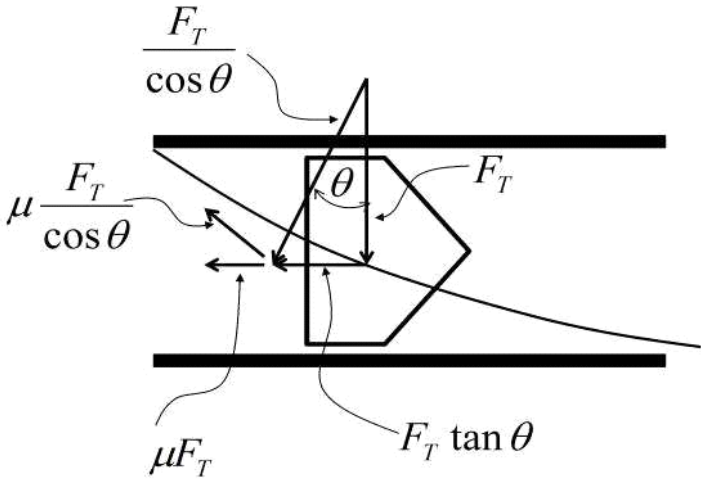

where *r* is the radius of the bore. Notice in the figure above that, in addition, projecting force $\frac{F_T}{\cos\theta}$ on the longitudinal direction gives rise to force $G_T = F_T \tan\theta$, which is an inertial force and also slows down the pellet movement. Since G_T is an inertial force, it is already accounted for in the expression for the pellet acceleration (this force is given by the term $(2\pi T_R)^2 I_b \frac{dv_b}{dt}$).

The friction force is therefore given by the expression

$$G = G_n + \mu p_b \pi D_b \delta_s + \mu \frac{4\pi T_R}{D_b} I_b \frac{dv_b}{dt} \qquad \text{(EQ 49)}$$

Replacing in the equation for the pellet acceleration and after some algebraic manipulations, the pellet acceleration is governed by the ODE,

$$\frac{dv_b}{dt} = \frac{A_b(p_b - p_n) - (G_n + \mu p_b \pi D_b \delta_s)}{m_b + 4\pi T_R I_b\left(\pi T_R + \frac{\mu}{D_b}\right)} \quad \text{(EQ 50)}$$

If the rifling lands are approximately equally smooth as the rifling grooves, the friction coefficient for the skirt and the rifling can be assumed to be the same.

Pressure on the pellet nose. In general, computing the pressure on the pellet nose amounts to solving a compressible fluid dynamic problem. You can get around this by making a simple assumption about the air flowing in the barrel ahead of the pellet. If the Mach number is small, you can treat this air as incompressible and get a simple formula for the nose pressure. This approximation is rather crude, but it should suffice to determine to what extent the inertia of the air ahead of the pellet is important (it is not significant, as you will see from numerical computations.) Under the assumption of very small Mach number you don't need the energy equation, and you can treat the cylinder of air filling the barrel ahead of the pellet as a slug whose length shortens as the pellet moves down the barrel.

If the barrel length is L_m and x_b is the position of the pellet in the barrel (you can assume the pellet dimensions are negligible compared with the barrel length), and assuming conditions ahead of the pellet are uniform, the momentum equation is as follows

$$(p_n - p_a)A_b = \frac{d}{dt}[A_b(L_m - x_b)\rho_a v_b] + (\rho_a v_b)A_b v_b \quad \text{(EQ 51)}$$

where subscript a refers to atmospheric conditions. The first term on the right is the rate of change of momentum inside the barrel, and the second term is the momentum flowing out the muzzle. This equation yields an expression for the nose pressure

$$p_n = p_a + (L_m - x_b)\rho_a \frac{dv_b}{dt} \quad \text{(EQ 52)}$$

If you use this expression as written, you must time-lag the pellet acceleration. Alternatively, you can now get an explicit equation for the nose pressure by clearing the pellet acceleration. Replacing $\frac{dv_b}{dt}$ in the equation above results in the following expression for the pellet nose pressure in terms quantities known at solution time,

$$p_n = \frac{\left[m_b + 4\pi T_R I_b\left(\pi T_R + \frac{\mu}{D_b}\right)\right]p_a + (L_m - x_b)\rho_a[A_b p_b - (G_n + \mu p_b \pi D_b \delta_s)]}{\left[m_b + 4\pi T_R I_b\left(\pi T_R + \frac{\mu}{D_b}\right)\right] + (L_m - x_b)\rho_a A_b} \quad \text{(EQ 53)}$$

5.2 Summary of differential equations

With n finite elements to discretize the spring, the internal ballistics problem of a spring airgun is described by a set of $n+4$ coupled ordinary differential equations.

Spring finite element equations

Shown here for the case of four finite elements,

$$\frac{\mathrm{d}}{\mathrm{d}t}\begin{bmatrix} v^1 \\ v^2 \\ v^3 \\ v^4 \end{bmatrix} = \begin{bmatrix} -2\zeta & \zeta & 0 & 0 \\ \zeta & -2\zeta & \zeta & 0 \\ 0 & \zeta & -2\zeta & \zeta \\ 0 & 0 & \zeta & -\zeta_M \end{bmatrix}\begin{bmatrix} x^1 \\ x^2 \\ x^3 \\ x^4 \end{bmatrix} + \begin{bmatrix} \zeta x_0 - \mathrm{sgn}(v^1)\dfrac{F_f^1}{m} \\ -\mathrm{sgn}(v^2)\dfrac{F_f^2}{m} \\ -\mathrm{sgn}(v^3)\dfrac{F_f^3}{m} \\ \zeta_M \Delta - \mathrm{sgn}(v^4)\dfrac{F_f^4 + F}{M} \end{bmatrix} \tag{EQ 54}$$

Density, temperature, and pressure in compression chamber

$$\frac{\mathrm{d}\rho_c}{\mathrm{d}t} = \frac{-C_d \eta \dot{m} + \rho_c v_p}{L + \delta - x_p} \tag{EQ 55}$$

$$\frac{\mathrm{d}T_c}{\mathrm{d}t} = \frac{p_c v_p - C_d \eta \dot{m}\left(\frac{1}{2}v_d^2 + c_p T_d - c_v T_c\right) - \frac{1}{A_p}\frac{\mathrm{d}Q}{\mathrm{d}t}}{(L + \delta - x_p)\rho_c c_v} \tag{EQ 56}$$

$$p_c = \rho_c R T_c \tag{EQ 57}$$

Heat loss in compression chamber

$$\frac{\mathrm{d}Q}{\mathrm{d}t} = \mu\left[\pi D_p (L - x_p) + \frac{\pi}{4}D_p^2\right](T_c - T_a) \tag{EQ 58}$$

Density, temperature, and pressure in barrel between breech and pellet

$$\frac{\mathrm{d}\rho_b}{\mathrm{d}t} = \frac{C_d \eta_b \dot{m} - v_b \rho_b}{x_0 + x_b} \tag{EQ 59}$$

$$\frac{dT_b}{dt} = \frac{C_d \eta_b \dot{m}\left(c_p T_d - c_v T_b + \frac{1}{2} v_d^2\right) - p_b v_b - \frac{1}{A_b}\frac{d}{dt}KE - \frac{1}{A_b}\frac{dQ_b}{dt}}{(x_0 + x_b)\rho_c c_v} \quad \text{(EQ 60)}$$

$$p_b = \rho_b R T_b \quad \text{(EQ 61)}$$

Heat lost in barrel

$$\frac{dQ_b}{dt} = \mu \pi D_b x_b (T_b - T_a) \quad \text{(EQ 62)}$$

Kinetic energy in barrel between breech and pellet

This term has a relatively small impact on the solution and can be safely computed by time-lagging. Remember this kinetic energy calculation is approximate and not fully consistent with our uniformity assumptions.

$$KE = \frac{1}{6} A_b \rho_b [v_b^2 + v_0 (v_b + v_0)] x_b + \frac{1}{2} A_b \rho_b x_0 v_0^2 \quad \text{(EQ 63)}$$

Pellet motion equation

$$\frac{dv_b}{dt} = \frac{A_b (p_b - p_n) - (G_n + \mu p_b \pi D_b \delta_s)}{m_b + 4\pi T_R I_b \left(\pi T_R + \frac{\mu}{D_b}\right)} \quad \text{(EQ 64)}$$

Pellet nose pressure

$$p_n = \frac{\left[m_b + 4\pi T_R I_b \left(\pi T_R + \frac{\mu}{D_b}\right)\right] p_a + (L_m - x_b)\rho_a [A_b p_b - (G_n + \mu p_b \pi D_b \delta_s)]}{\left[m_b + 4\pi T_R I_b \left(\pi T_R + \frac{\mu}{D_b}\right)\right] + (L_m - x_b)\rho_a A_b} \quad \text{(EQ 65)}$$

You can solve this system using a conventional finite difference technique, the simplest one being the Euler scheme.

6.0 Results and discussion

6.1 Validation

The internal ballistics model was validated on a 4.5 mm caliber Beeman RS2 air rifle using four high-quality lead pellets manufactured by JSB in the Check Republic. The pel-lets weights were 0.510 g (7.87 gr), 0.547 g (8.44 gr), 0.670 g (10.34 gr), and 0.870 g (13.43 gr). The first three pellets are favored by competitive shooters in the Field Target discipline, and the fourth is preferred for hunting.

The Beeman RS2 is an inexpensive airgun whose barrel can be easily removed. To get data of pellet velocity as a function of barrel length, the gun barrel was successively cut off in six different lengths, and muzzle velocities were measured for each pellet. The shortest length of barrel that could be tested was dictated by mechanical constraints.

Table 1 shows the basic characteristics of the gun. I will refer to this table as the "benchmark gun configuration". Some of the measurements were made in imperial units and translated into metric units, which explains the apparent excessive number of digits in the metric numerical values. The piston friction force was measured with a trigger weight gage at about 72 ounces (2.041 Kg). There was no measurable friction force associated with the spring guide. The chamber compensation depth was arrived at by computing the volume of a 2 mm deep, 1 mm wide, circular groove in the parachute seal. The breech gap (seating depth) was measured at about 0.5 mm.

TABLE 1. Beeman RS2 action technical specifications.

Spring			Piston			Chamber		
Free length	285.75	mm	Weight	0.298	Kg	Diameter	25	mm
Number coils	43	----	Piston head thickness	12	mm	Seal cavity comp. depth	0.53	mm
Outside diameter	17.78	mm	Seal thickness	6.7	mm	Transfer port diameter	3.4	mm
Wire diameter	3.02	mm				Transfer port length	23	mm
Spring precompression	52.705	mm						
Rear spacer thickness	0	mm						
Front spacer thickness	7.49	mm						
Cocking stroke	100	mm						
Guide length	100	mm						

The next table shows the average of measured muzzle velocities, and their respective standard error. A standard electronic chronograph was used, with the shots fired from a distance of about 0.2 m. In most cases the number of shots fired for each barrel length and pellet weight was from 15 to 20. The barrel lengths in Table 2 are metric translations of 4, 6, 8, 10, 12, and 14 inches. Since there is no practical way to know what the intrinsic variability of the chronograph is, the standard errors in Table 2 only account for the variability of measured velocities.

TABLE 2. Muzzle velocity estimations and standard errors for four JSB 4.5 mm lead pellets.

	Estimated muzzle velocities (m/sec)				Estimators standard error (m/sec)			
P. weight (g) / B. length (m)	0.510	0.547	0.670	0.870	0.510	0.547	0.670	0.870
0.1016	233	226	210	178	0.3	0.4	0.2	0.4
0.1270	249	244	225	194	0.3	0.2	0.2	1.2
0.2032	268	261	234	199	0.5	0.4	0.3	0.5
0.2540	277	266	240	204	0.4	0.6	0.2	0.6
0.3048	274	267	242	206	0.3	0.5	0.6	0.8
0.3556	275	267	246	215	0.9	0.4	0.2	0.4

Model parameters estimation. In this model there are only two parameters that cannot be measured and must be calibrated. These are the skirt friction coefficient and the heat transfer coefficient. All other parameters can be measured. Table 3 shows the measured parameters - these quantities were measured using a trigger gage. Some of the parameters in Table 3 are pellet-dependent and others are not. To measure the bearing depth of the skirt, which is defined as the depth of the skirt that comes into close contact with the barrel as a result of high pressure deformation, pellets were shot into a box filled with soft tissue paper and recovered with minimal deformation. The bearing depth of the skirt was approximately measured at 1.2 mm for the lighter pellets, and was observed to be slightly shorter for the heavier pellets. However, for the purpose of calculation, the skirt depth was assume to the same for all pellets. This is not a problem since the skirt friction coefficient can be adjusted to account for any difference in skirt depth.

TABLE 3. Measured model parameters for four JSB 4.5 mm lead pellets.

	Pellet weight (g)			
Measured parameter	0.510	0.547	0.670	0.870
Skirt bearing depth (mm)	1.2	1.2	1.2	1.2
Elastic friction force (Kg)	0.544	0.544	0.227	0.227
Breaking force (Kg)	2.722	2.722	1.814	1.814
Piston seal force (Kg)	2.041	2.041	2.041	2.041
Breech gap (mm)	0.5	0.5	0.5	0.5

A rigorous calibration procedure for the skirt friction and heat transfer coefficients would entail a non-linear optimization problem for each pellet. Rather than embarking on an extensive numerical computation exercise, a simplified calibration only considering the skirt friction coefficient was carried out, by matching the velocities corresponding to the longest barrel.

In all the computations that follow, the finite element discretization of the spring involved 40 finite elements of equal length.

The calibrated skirt friction coefficients are shown in the Table 4.

TABLE 4. Skirt friction coefficient calibrated to match muzzle velocities for four JSB 4.5 mm lead pellets and 0.3556 m (16 in) barrel.

	Pellet weight (g)			
Calibrated parameter	0.510	0.547	0.670	0.870
Skirt friction coefficient	0.349	0.343	0.323	0.305
Heat transfer coefficient	0.000	0.000	0.000	0.000

Using the coefficient values in Table 4, muzzle velocities where computed for the other barrel lengths and compared with measurements. As indicated in the figures below, the velocities for all barrel lengths are matched reasonably well with the skirt friction coefficient alone, and there is no need for heat transfer.

This doesn't mean the process is entirely adiabatic, what it means is that there is some colinearity between skirt friction and heat transfer. For practical purposes, however, these results indicate that an adiabatic process captures the most important physics.

It is relatively easy to make sense of the calibrated values in Table 4. The two lighter pellets are similar to each other in that both have pronounced waists and relatively thin skirts. Their noses offered more resistance to movement inside the barrel than the two heavier ones. The two heavier ones are also similar to each other, but significantly different from the two lighter ones. The two heavier pellets had thicker skirts, much less pronounced waists, and offered less resistance when driven into the barrel. A pellet with a thinner, more compliant skirt will experience more of its friction from the skirt, both because of easier deformation under pressure, and because of a larger bearing area. The fact that the skirt depth was assumed to be the same for all pellets only reinforces this idea.

TABLE 5. Assumed axial moments of inertia as fractions of uniform cylinder moment of inertia.

Pellet mass (g)	0.510	0.547	0.670	0.870
Cylinder moment of inertia (kg m^2)	1.29E-09	1.38E-09	1.69E-09	2.20E-09
Fraction	0.9	0.9	0.9	0.9
Assumed moment of inertia (kg m^2)	1.16E-09	1.24E-09	1.52E-09	1.98E-09

FIGURE 9. Computed versus experimentally estimated muzzle velocities for four 4.5 mm JSB match quality pellets - notice the expanded vertical scales.

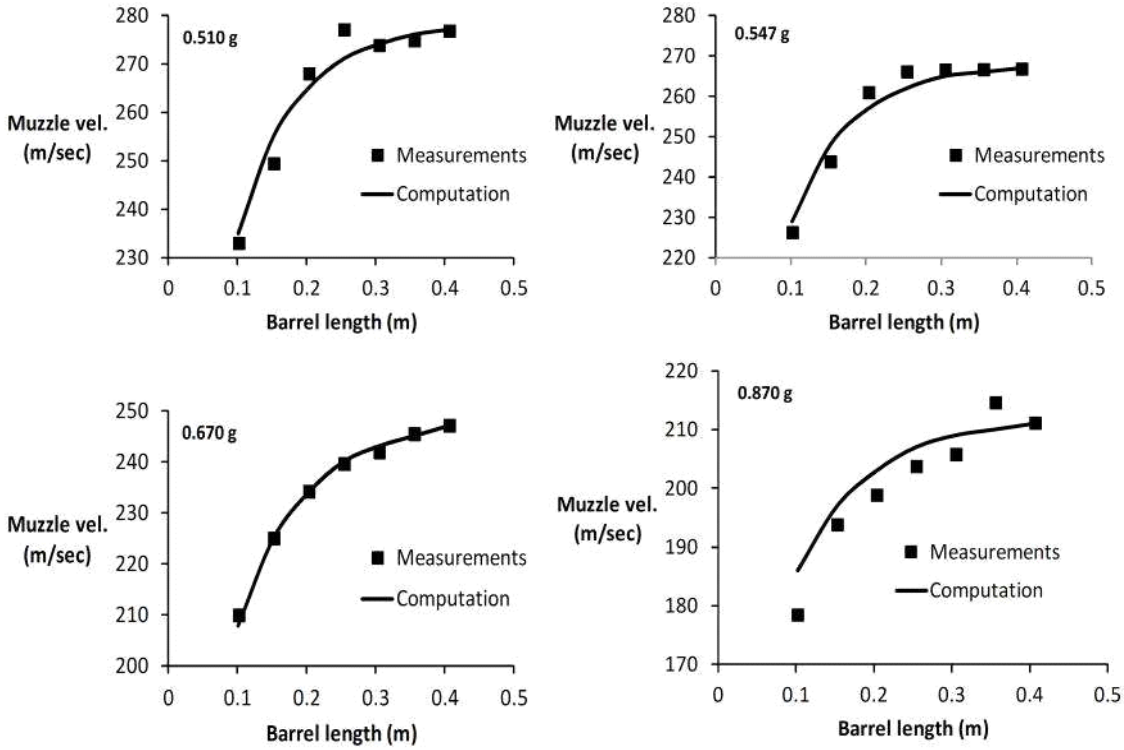

Figure 9 shows the level of agreement this model gives us with just calibration parameter for each pellet. In the case of the 0.670 g (10.34 gr) pellet the agreement between computation and experiment is exceptionally good. Given the uncertainty in the measurement equipment, and given the relatively modest quality of the gun, this level of agreement is very satisfactory.

It would be straightforward but somewhat laborious to compute the moment of inertia of the pellets used. Therefore, a simple approximation was used by assuming the moment of inertia of each pellet to be 90% of the moment of inertia of a cylinder of the same mass and diameter as the pellets, as shown in the next table.

Granted that this is a simplistic assumption, but as I will discuss in the next section, the rotational energy due to barrel twist has a very small impact on performance and there is not much to gain from an accurate calculation of the pellet's axial moment of inertia.

This level of agreement gives us reassurance the model captures the essential physics. Let's now use the model to gain insights into the internal dynamics of a spring piston air-gun.

FIGURE 10. Typical firing cycle for the Beeman RS2 air rifle with the 0.670 g JSB pellet, 0.3556 m (16 in) barrel (distances not to scale).

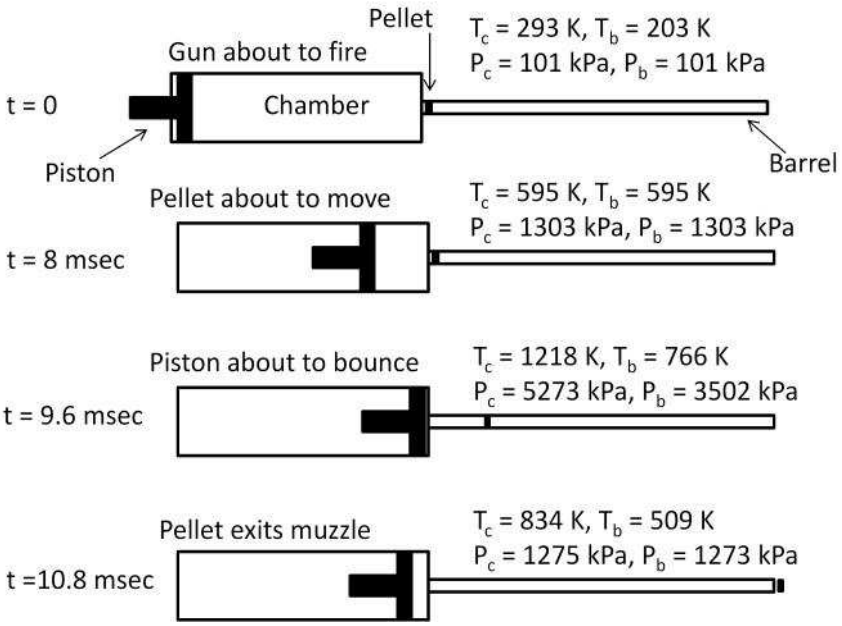

6.2 Firing cycle

Figure 10 shows a stylized airgun action arrangement during a typical firing cycle. The gun is fired under atmospheric conditions. Pressure and temperature in the chamber rise (adiabatically and isentropically in this case) until the breaking force (1.814 kg in this case) is reached at the breech and the pellet begins to move. When the pellet has travelled a distance somewhat less than a fourth of the barrel length, the piston bounces backwards and the pellet continues its travel down the barrel.

Peak temperatures and pressures occur during pellet travel in the bore and are significantly higher than the corresponding values at bounce time. The highest chamber pressure and temperature are 29,248 kPa and 1452 K, respectively, while the highest values for the breech are 27,298 kPa and 1,506 K.

Computations suggest there are three possible regimes that describe a spring-piston airgun firing cycle.

Smooth piston bounce. This occurs when the piston seal reaches almost to the end of the chamber and bounces backwards without touching the end of the chamber. In this regime, the piston bounces on a cushion of high pressure air. The pellet begins movement shortly before the piston bounces.

Piston bounce after collision. This appears to be the most common situation. The piston reaches the end of the chamber, makes physical contact with the end of the chamber, and bounces backwards. As in the previous case, the pellet begins movement shortly before the

piston reaches the end of the chamber. In this regime the kinetic energy of the piston is dissipated in the collision with the end of the chamber.

Piston collides but does not bounce. In this case the piston seal collides with the end of the chamber and the pellet exits the muzzle before the piston bounce starts.

Transfer port Mach number. The discharge transfer port Mach number was found to be always less than one, as illustrated in Figure 11. This doesn't mean the air speed out of the transfer port was low, since the speed of sound in the transfer port is much higher than under atmospheric conditions. From an efficiency point of view, subsonic discharge is much better than super-critical flow. The following figure shows the evolution of transfer port Mach number for the benchmark case.

The standard definition of Mach number is unsigned. However, in order to bring up the flow direction through the transfer port, the plot shows a signed version of Mach number, where negative values correspond to flow reversal from the breech into the compression chamber. Notice that the Mach number is relatively low throughout the firing cycle.

FIGURE 11. Transfer port Mach number (0.670 g JSB pellet, 0.3556 m barrel).

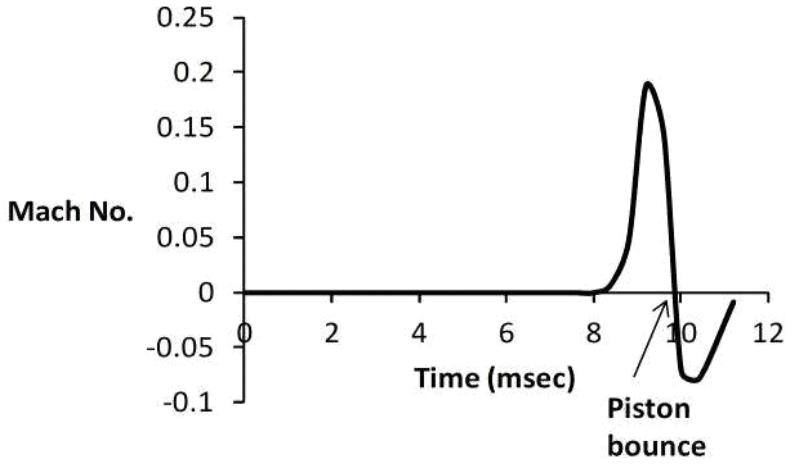

Pressure and temperature during firing cycle. Figure 12 shows the evolution of temperature and pressure during firing. Notice that the pressures in the chamber and breech are almost indistinguishable - the reason for this is that the discharge through the transfer port is always subsonic. In contrast, the temperatures in the chamber and breech are close, but not identical. The difference arises primarily from non-isentropic mixing in the breech.

FIGURE 12. Temperature and pressure during firing cycle (0.670 g JSB pellet, 0.3556 m barrel).

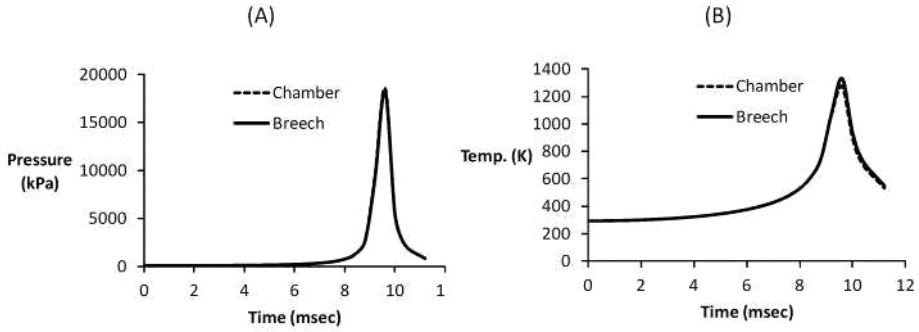

Piston and pellet velocities during firing. Closely looking at the piston velocity during the firing cycle helps us visualize the difference between the standard spring model, where the piston mass is corrected to account for the mass of the spring, and the finite elements approximation of the spring, which properly captures the distributed spring mass. The following figure compares the piston velocity for these two cases (0.670 g JSB pellet.)

FIGURE 13. Piston velocity during firing - standard mass-corrected versus finite elements spring model (0.670 g JSB pellet, 0.3556 m barrel.)

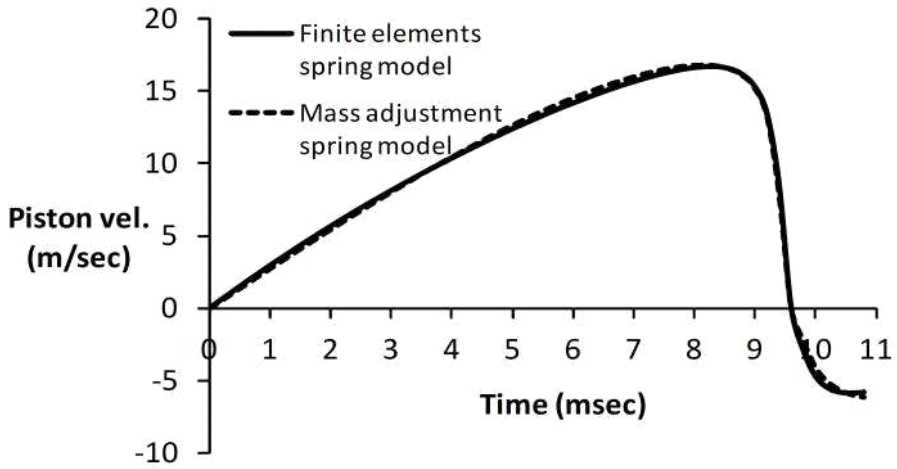

Although the two curves follow each other closely, the finite elements model leads to a slightly lower power output (approximately 1 Joule, or about 6 m/sec). This difference is attributable to the higher retention of both kinetic and elastic energy in the case of the finite element model. In fact, while the spring in the mass-compensated model loses about 85% of its energy in the firing cycle, the spring in the finite element model loses about 78% of its energy. Keep in mind that these two models would be equivalent under uniform spring deflection. The spring in an airgun doesn't deflect uniformly, however, especially towards the end of the firing cycle when impact against the chamber end wall excites longitudinal vibration in the spring.

Figure 14 shows the velocity of the spring and the pellet. Notice that by the time the piston bounces back, the pellet has accelerated to approximately 50% of its muzzle velocity.

FIGURE 14. Piston and pellet velocities (0.670 g JSB pellet, 0.3556 m barrel.)

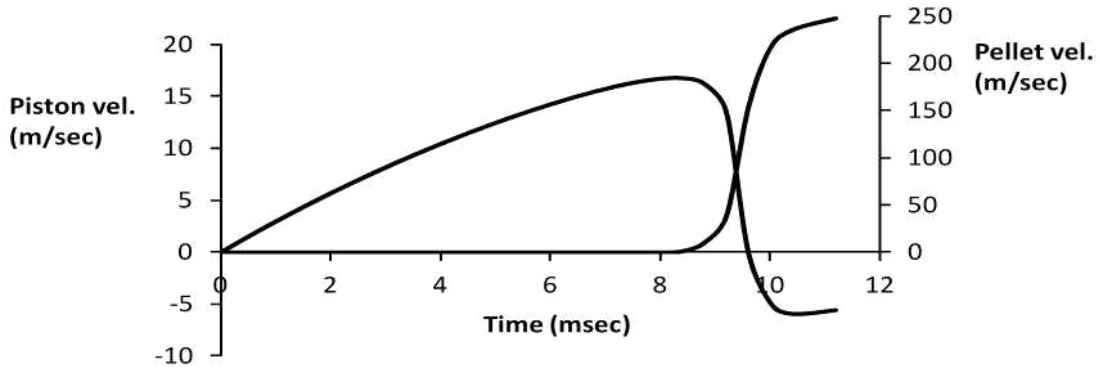

FIGURE 15. Energy balance during firing cycle (0.670 g JSB pellet, 0.3556 m barrel) - EE stands for elastic energy, KE stands for kinetic energy, and TE stands for thermal energy.

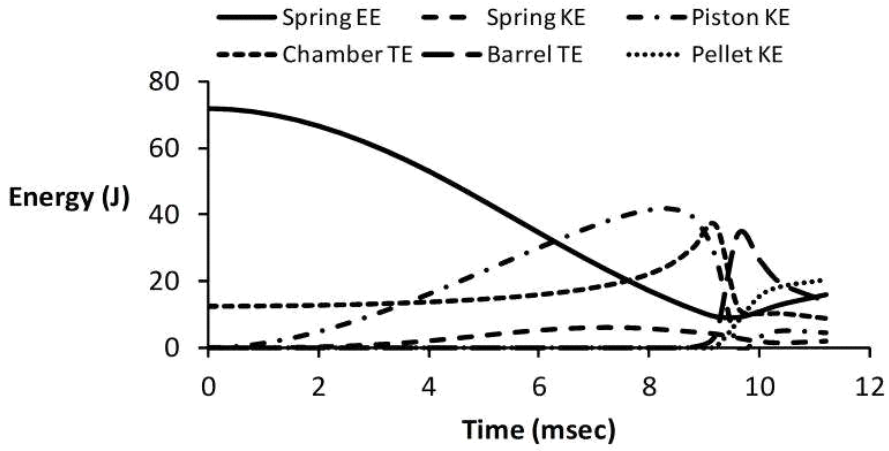

6.3 Energy budget and balance

When the gun is cocked and before the firing cycle stars, the vast majority of the energy is stored in the compressed spring in the form of elastic energy, and some energy is also present in the form of thermal energy in the compression chamber, the transfer channel, and the breech gap. During the firing cycle, a complex process of energy exchange occurs between the spring, the compression chamber, the volume of air behind the pellet, and the pellet itself.

Figure 15 shows the energy exchange during the firing cycle. Besides energy exchanges within the gun, energy is also expelled from the gun in the form of kinetic energy imparted to the projectile, friction and heat dissipation, as well as enthalpy flows out of the muzzle while the pellet is travelling inside the barrel, and enthalpy outflow through the back of the action when the piston recedes during bouncing. If all the sources and losses of energy are taken into account, the total energy budget must remain constant. The following table shows the detailed energy budget right before the gun is fired and immediately after the pellet leaves the barrel. As you can see, the energy budget remains constant to less than one hundredth of one percent of the initial energy in the spring. The small difference of 0.0033 Joules is due to numerical truncation error in the integration of the ODE system, and to some extent is also due to the inconsistency in imposing a linearly varying velocity behind the pellet.

TABLE 6. Energy budget at the beginning and end of firing cycle (fractions are with respect to the initial elastic energy of the spring) for the relevant airgun components (0.670 g JSB pellet, 0.3556 m barrel.)

Energy Balance (Joules)					
Comp	Energy	Start	Finish	Diff	Fraction
Spring	Elastic	71.79	16.09	-55.70	-77.6%
	Kinetic	0.00	1.97	1.97	2.7%
	Guide	0.00	0.00	0.00	0.0%
	Total	71.79	18.06	-53.73	-74.8%
Piston	Kinetic	0.00	4.47	4.47	6.2%
	Impact	0.00	6.75	6.75	9.4%
	Friction	0.00	2.17	2.17	3.0%
	Outflow	0.00	-4.57	-4.57	-6.4%
	Total	0.00	8.82	8.82	12.3%
Chamber	Thermal	12.46	8.81	-3.65	-5.1%
	Transfer	0.05	0.45	0.40	0.6%
	Heat loss	0.00	0.00	0.00	0.0%
	Total	12.51	9.26	-3.25	-4.5%
Breech to pellet	Thermal	0.00	13.96	13.96	19.4%
	Kinetic	0.00	0.13	0.13	0.2%
	Heat loss	0.00	0.00	0.00	0.0%
	Total	0.00	14.09	14.09	19.6%
Muzzle	Outflow	0.00	0.84	0.84	1.2%
	Total	0.00	0.84	0.84	1.2%
Pellet	Linear KE	0.00	20.47	20.47	28.5%
	Rot KE	0.00	0.01	0.01	0.0%
	Friction	0.00	12.76	12.76	17.8%
	Total	0.00	33.24	33.24	46.3%
			Net energy change	-0.0033	0.0%

Close examination of this table sheds light on the inefficiencies of a typical airgun. Only about 28% of the spring initial energy converts to kinetic energy of the projectile. Almost

18% of the spring energy is lost to overcoming the pellet friction in the barrel, about 19% (almost the same amount) remains as thermal energy behind the pellet at exit time, and about 22% is retained by the spring as deformation energy. Notice that the rotational energy is insignificant in comparison to the other components.

6.4 Simple parametric analysis

Performance sensitivity to design parameters can yield useful insights into what an optimally designed spring powered airgun may look like. Of the many parameters you can analyze, I will focus on the compression chamber diameter, the transfer port diameter, and the transfer channel length.

Effect of chamber diameter. The following figure illustrates the effect of chamber diameter on pellet power for two popular JSB pellets for the benchmark gun configuration.

FIGURE 16. Effect of compression chamber diameter on power output (0.547 g and 0.670 g JSB pellets, 0.3556 m barrel.)

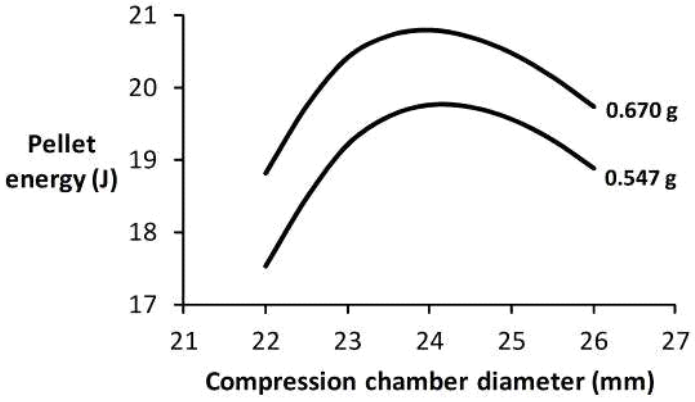

Two things stand out in this figure. The optimal chamber diameter appears to be slightly greater than 24 mm, and slightly greater yet for the lighter projectile. The actual chamber diameter is 25 mm. A more refined calculation that took into account the change in piston weight as a function of chamber diameter would tend to move the optimal value to the right. The reason is that power output sensitivity to piston weight, in the vicinity of the design parameters of this rifle, is positive. Computations show that, at the margin, an increment of one gram in piston weight leads to an increment of about 0.047 Joules in power output for the 0.547 g pellet. Since increasing the chamber diameter would also lead to a heavier piston, the optimal values shown in the figure above are biased low. This is reassuring in that the Beeman RS2 appears to have a nearly optimal chamber diameter.

Effect of transfer port diameter. This is a parameter that can be varied relatively independently of other design constraints. Of the two figures below, figure (A) is for the design conditions of the Beeman RS2, where the transfer channel is 23 mm in length. According to the figure, the optimal transfer port diameter is about 3 mm for the 0.670 g pellet, and slightly less for the 0.547 g pellet. The actual transfer port diameter is 3.4 mm.

Although there is no way to know if the Beeman RS2 transfer port was designed optimally, you can argue that the optimal values shown in the figure are biased low. The reason is that these computations were done under a discharge coefficient equal to one. Under a discharge coefficient slightly smaller than one, the effective port diameter would be larger and the optimal value would be displaced to the right.

FIGURE 17. Effect of transfer port diameter on pellet energy for two JSB pellets - figure on the left is for the nominal transfer channel length of 23 mm, figure on the right is for the 0.670 g JSB pellet and varying transfer channel lengths.

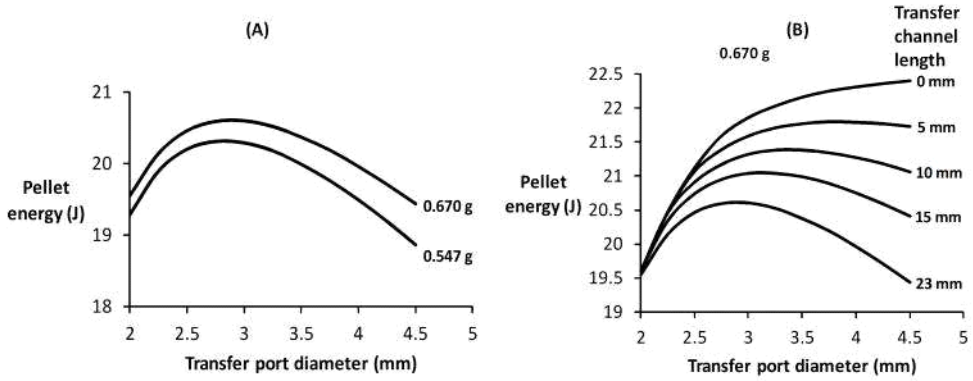

In the figure above, figure (B) shows the effect of port diameter for varying channel lengths. If the channel length is zero, namely if the volume of the transfer channel is zero, the optimal transfer port diameter matches the diameter of the breech. This result is expected since matching the breech diameter means there is no entropic mixing of the air as it exits the compression chamber.

Effect of transfer channel length. This essentially amounts to another view of Figure 16 (B). Since the transfer channel is basically dead space in the compression chamber, with some caveats, it is intuitively clear that in the absence of complicating issues such as the vena contracta effect, minimizing the transfer channel length maximizes power yield.

The next figure shows the effect of transfer channel length. There is an almost linear relationship between transfer channel length and power output. This is expected from first principles - the transfer port channel influences power yield through its volume, which can be viewed as a perturbation on the chamber volume. If the vena contracta effect were taken into account, the line in Figure 17 would show a less steep slope as it approaches zero, and perhaps even a maximum - this question can't be settled without additional research. In view of this we can argue that computations probably overestimate the effect on power of a decrement in transfer port size.

FIGURE 18. Effect of transfer channel length (0.670 g JSB pellet, 0.3556 m barrel.)

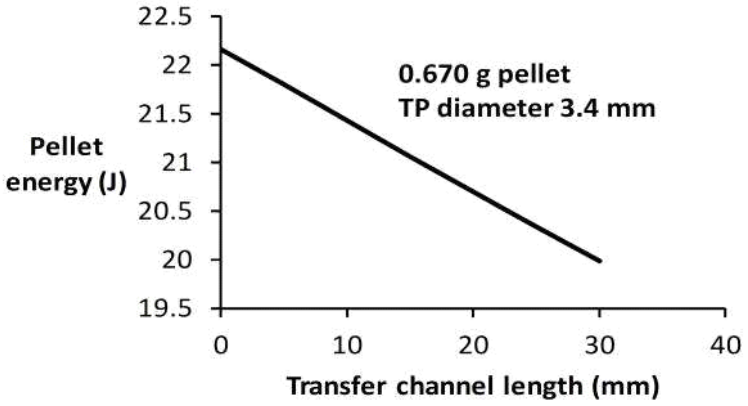

7.0 Conclusions

I described and validated a comprehensive model for the internal dynamics of spring piston airguns, where the thermodynamic effects are modelled as quasi-stationary from a fluid dynamics point of view. The model successfully describes the complexities of energy balance between the various components of the airgun action, and is significantly more comprehensive than others in the open literature in that the current approach accounts for details of practical importance, such as cavities in the seal face and volume of transfer channel. The model was successfully calibrated under adiabatic assumptions to measured velocities of four common high quality pellets, fired from a standard medium power air rifle. It is important to keep in mind the substantial underlying assumptions of this model, however. Those assumptions, notably the neglecting of kinetic energy in the compression chamber at a time when the piston is quickly approaching the end of its stroke, would have to be tested against a full Navier Stokes model of the chamber gas dynamics.

8.0 References

1. S.J. Compton, “Internal ballistics of a spring-air pellet gun”, Internet paper, May 2007
2. C.E. Mungan, “Internal ballistics of pneumatic potato cannon”, Eur. J. Phys. 30, -457, 2009
3. M. Denny, “The internal ballistics of an air gun”, The Physics Teacher, 49, 181-183, Feb. 2011
4. Z. J. Rohrbach,T. R. Buresh, and M.J. Madsen, “Modeling the exit velocity of a compressed air cannon”, Am. J. Phys. 80 (1), 24-26, Jan. 2012
5. L. Ruby, “Equivalent mass of a coil spring”, The Physics Teacher, 38, 148-149, March 2000
6. A.D. Deutschman, WJ Michaels, and C.E. Wilson, “Machine Design - Theory and Practice”, Mcmillan, 757-758, 1975

7. D.E. Carlucci and S.S. Jacobson, “Ballistics - Theory and design of guns and ammunition”, CRC Press, 64-96, 2008
8. W.F. Morrison, G. P. Wren, W.F. Oberle, and S.L. Richardson, “The Application of Lagrange and Pidduck-Kent Gradient Models to Guns Using Low Molecular Weight Gases”, ARL-TR-48, February 1993